Supporting information

Metal Organic Frameworks as potential shock absorbers: case of the highly flexible MIL-53(Al)

Pascal G. Yot, Zoubeyr Boudene, Jasmine Macia, Dominique Granier, Louis Vanduyfhuys, Toon Verstraelen, Veronique Van Speybroeck, Thomas Devic, Christian Serre, Gérard Férey, Norbert Stock and Guillaume Maurin

1. Mercury intrusion

1.1. Phase transition determination

Mercury intrusion usually employed to determine the porosity, the pore size and the particle size distributions [1] has been successfully used to study the mechanical property of the MIL-53(Al) MOF material as demonstrated recently for MIL-53(Cr) and MIL-47(V^{IV}) [2, 3]. Considering the pore size of MIL-53(Al) ~0.85 nm and the pressure range accessible by the Hg porosimeter Micromeritics Autopore 9240 (P≤350 MPa)) the non-wetting mercury cannot penetrate into the pores, hence the pressure increase induces an isostatic pressure on the crystallites. The volume of intruded mercury is then directly related to the volumetric strain corresponding to the compressibility of the material. The powder was previously activated under secondary vacuum at 250°C during 8 h to obtain the large pore version of the MIL-53(Al): S.G. *Imcm*, V=1423.8(1) $Å^3$. The isostatic compression experiments were performed on activated powdered MIL-53(Al) samples outgassed at ~6.5 Pa during 4 h. The pressure applied can vary from 0.1 to 350 MPa. In the explored range of pressure, using the Washburn's law $P = -\frac{4\gamma\cos\theta}{d}$ with γ mercury surface tension and θ the contact angle of 0.485 N/m and 130° respectively, the pore diameters range in the interval [2×10^7–420 Å]. Cumulative and incremental volumes of intruded mercury have been reported as a function of the applied pressure with the aim at determining the effective pore diameter corresponding to the increase of volume in the range 13-18 MPa (Figure S1).

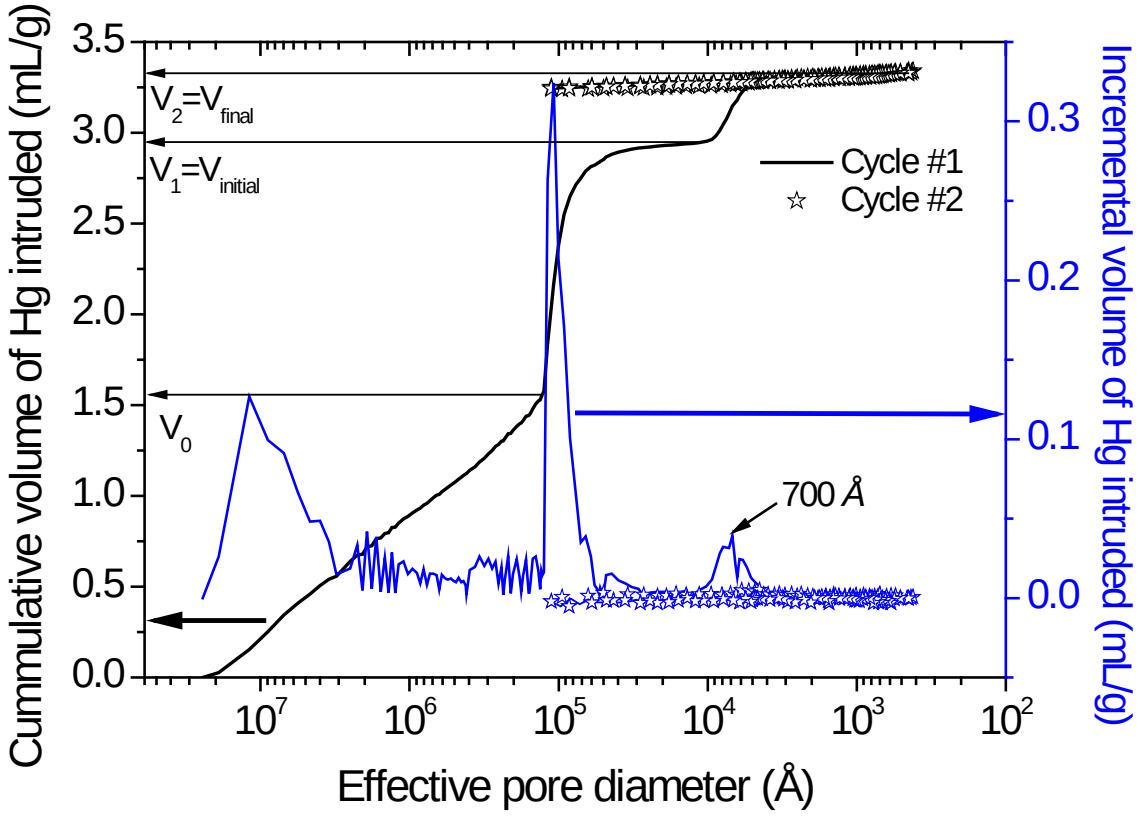

Figure S1 – Cumulative and incremental volumes of intruded mercury as a function of the effective pore diameter.

The mercury intrusion curve (in black) exhibits three different regions: (i) below ~10^5 Å (~2 MPa) where the intruded mercury ($V<V_0$) compacts the powder in the penetrometer, (ii) from ~10^5 to ~8×10^4 Å (~2 MPa to ~7 MPa) where the increase in volume (V_1-V_0) corresponds to the filling of inter-particular porosity, and (iii) after 104 Å (~13 MPa) corresponding to a sudden increase of the volume of intruded Hg. The variation of volume: V_2-V_1 corresponds to the shrinkage of the porous solid during the phase transformation used to estimate the volume of the closed pore form.

1.2. Particle size determination

Volumes of mercury related to the steps obtained upon pressure increase and decrease correspond to pore diameters of ~10^5 Å and ~700 Å respectively that are much larger than the window size of the MIL-53(Al) in its large pore form. It confirms that the step observed on the mercury intrusion curves is only the result of the plastic deformation of the powder particles.

The particle size distribution can be estimated using Mayer and Stowe's method [4]. The Mayer-Stowe equation, $P=\frac{\kappa\times\gamma}{Dp}$, was applied in the range of pressures, 0.2-10 MPa, corresponding to the filling of the interparticle voids by the mercury and allowed to determine the particles diameter distribution. The dimensionless Mayer-Stowe constant κ, was taken as 10 [5, 6]. The average particle diameter was found to be close to Dp=3.63 μm, and the width of the distribution was ~1.24 μm. Figure S2 summarizes the as calculated differential particle size distribution.

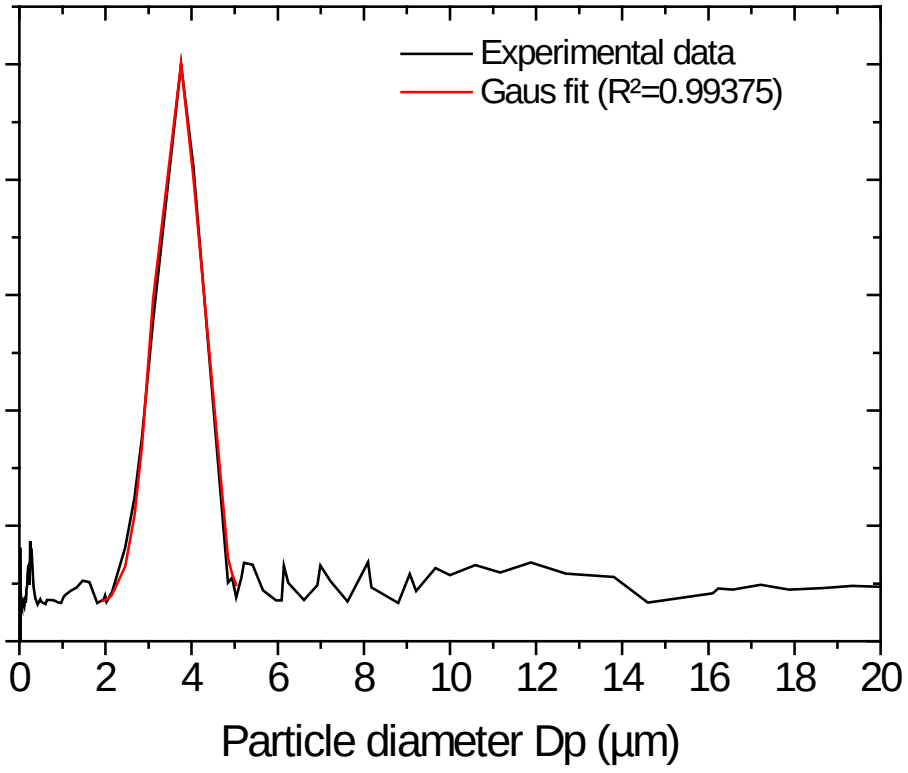

Figure S2 – Particle size distribution for MIL-53(Al) powder.

1.3. Bulk modulus estimation

The bulk modulus K of the two phases can be also estimated form the mercury intrusion curve using equation 1.

$$K_i = V_i\left(\frac{\partial P}{\partial V}\right) \qquad (1)$$

Where V_i is the volume of the initial phase, large pore or closed pore form. The bulk modulus is

then related to the slope of the linear domain of the mercury intrusion curve.

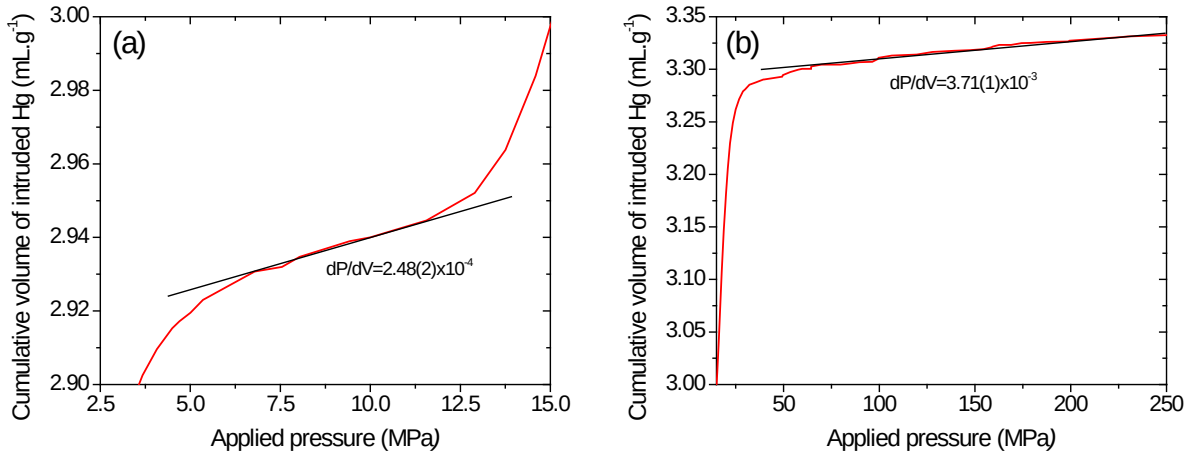

Figure S3 – Evolution of the volume of the powder as a function of the pressure in the domain corresponding to the large pore phase (a), closed pore phase (b) and estimation of the slope $\partial P/\partial V$.

1.4. Work estimation

The work corresponding to the phase transition can be roughly estimated using equation 2.

$$W = P\int_{V_1}^{V_2} dV \qquad (2)$$

Where V_1 and V_2 are the volumes of the large pore (1423.81 Å^3) and closed pore form (897.2(6) Å^3) respectively and P the pressure of transition 18 MPa.

2. Powder x-ray diffraction

Powder X-ray diffraction was performed on a PANalytical X'PERT II diffractometer using a monochromatic Cu-Kα source (λ=1.5406 Å) with operating voltage of 40 kV and a beam current of 40 mA. The patterns were collected for 2θ from 5° to 74°. Each powdered sample was introduced into a glass capillary tube of 0.5 mm diameter under argon atmosphere into a glove box and then sealed for the data acquisition. The unit-cell parameters were determined by indexing the X-ray powder patterns, using DICVOL06 followed by a Le Bail fit using FULLPROF [7, 8]. Figures S4 and S5 present the results of Le Bail fits for the initial large pore form and the form obtained after mercury intrusion respectively.

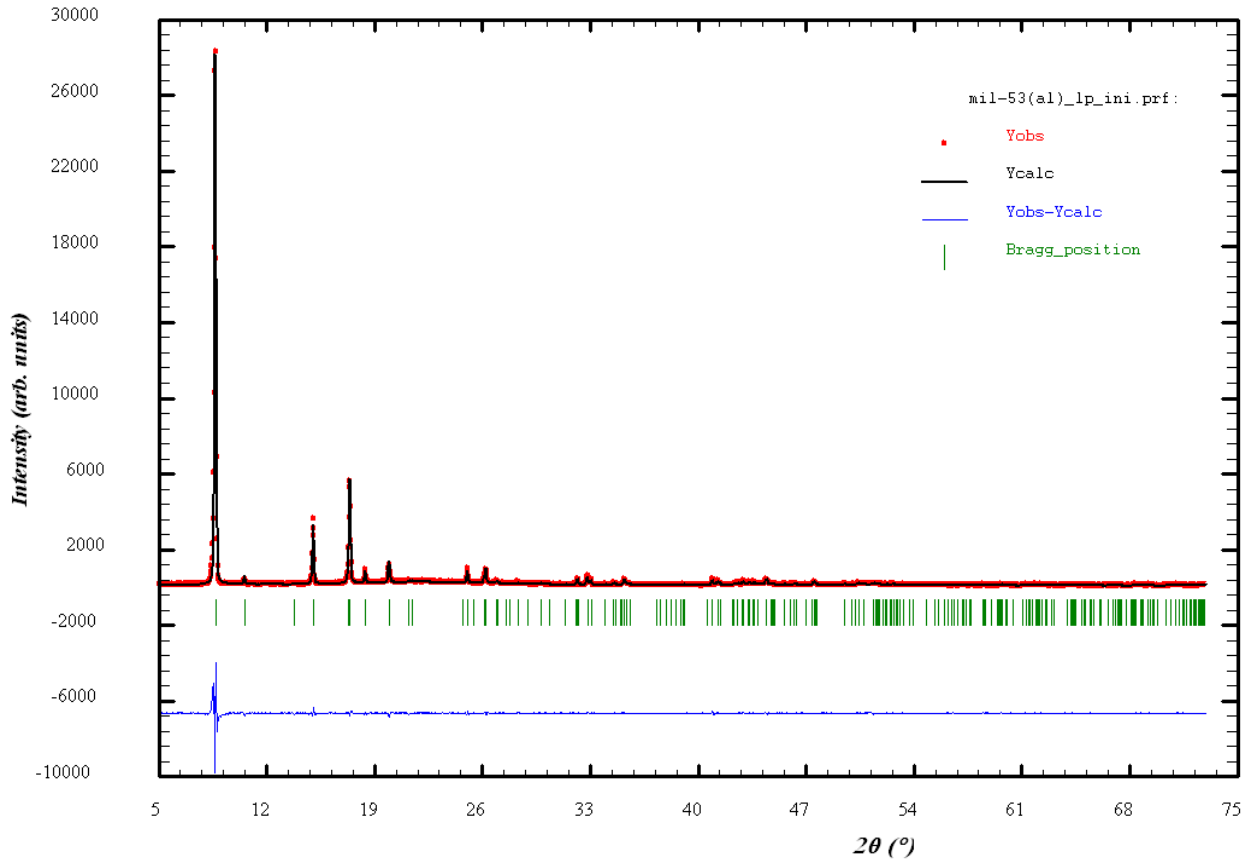

Figure S4 – Structure-independent refinements of the unit-cell of the diffraction pattern obtained for the activated powder before mercury intrusion experiment.

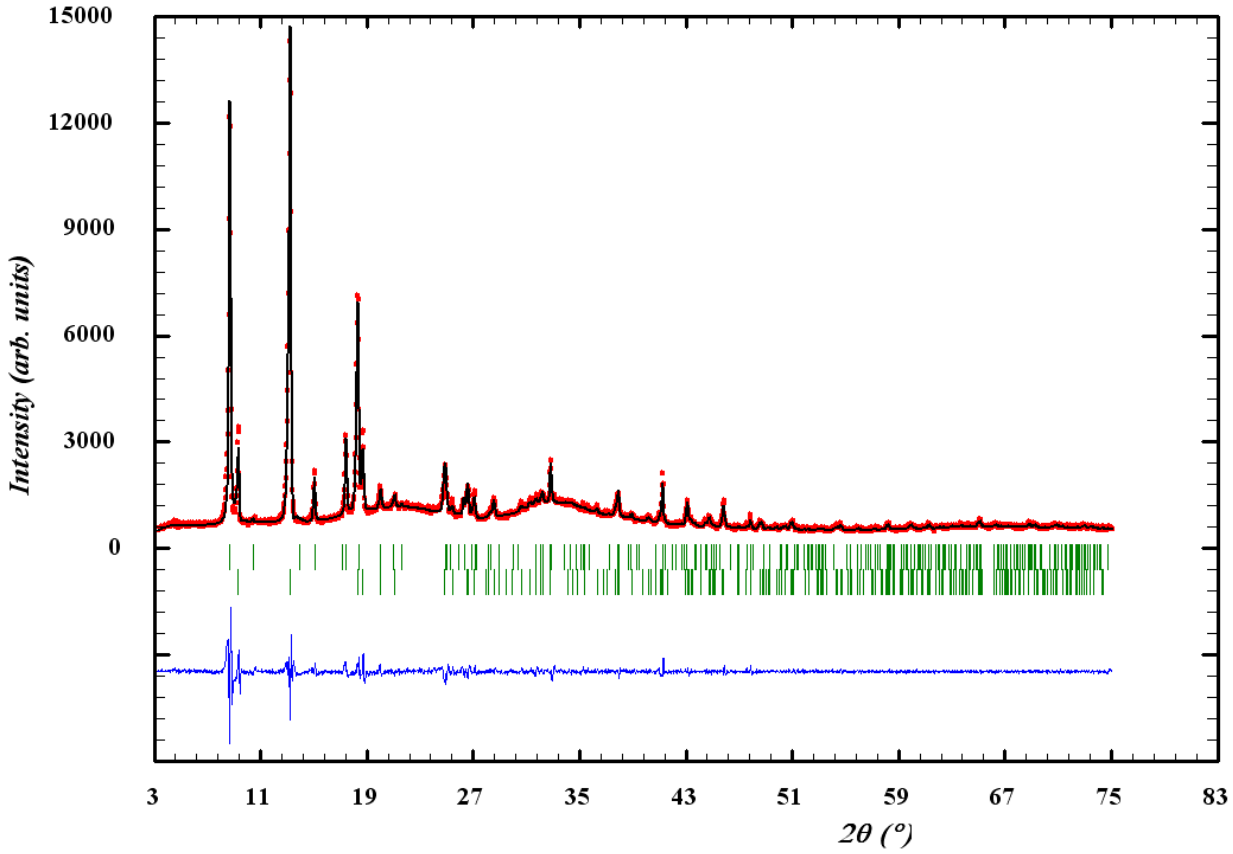

Figure S5 – Structure-independent refinements of the unit-cell of the diffraction pattern obtained for the powder after two cycle intrusion-extrusion.

	Space group	*a* (Å)	*b* (Å)	*c* (Å)	*β* (°)	*V* (Å^3)
Before compression experiment, activated powder	*Imcm*	16.732(1)	12.836(1)	6.629(2)	-	1423.8(1)
After compression experiment	*C2/c*	19.633(3)	7.160(1)	6.559(1)	104.70(1)	897.2(6)

Table S1 – Unit cell parameters obtained before and after mercury intrusion cycles.

The XRPD measurement was carried out after the mercury intrusion experiment on the powder collected into the penetrometer using a glove box (H_2O<1 ppm) to avoid rehydration of the porous solids. Nevertheless a longer time compared to the one in play during a mercury intrusion cycle (~2 h) has been required to prepare and further record the X-ray diffraction pattern (2 days). Such experimental conditions are most probably at the origin of the re-opening of the structure. However, the comparison between the intensities of the diffraction peaks corresponding to the LP and CP

forms suggests that the NP→LP conversion affects only a small fraction of crystallites. The relative high background observed in the pattern is due to mercury remaining present into the powder.

3. Micro-Raman scattering

Raman Scattering was carried out on a Horiba Jobin-Yvon Labram Aramis spectrometer working with 694 nm diode-laser. The pressure was generated with a diamond anvil cell (DAC), and was determined from the shift of the ruby R1 fluorescence line [9]. The DAC was under the 50× or 100× objectives of the Olympus microscope. A steel gasket with a hole of 120 µm in diameter and pre-indented to 55 µm thickness where the powder was loaded has been used. The powder was transferred into a glove box (H_2O <1 ppm) to avoid its rehydration. No pressure without transducer media was used to avoid overlapping signals from sample and pressure transmitting media. In addition, with the aim at eliminating the Raman peak of the diamond used in the DAC to generate the pressure spectra were recorded in two regions 50-1300 cm^{-1} and 1400-2100 cm^{-1}.

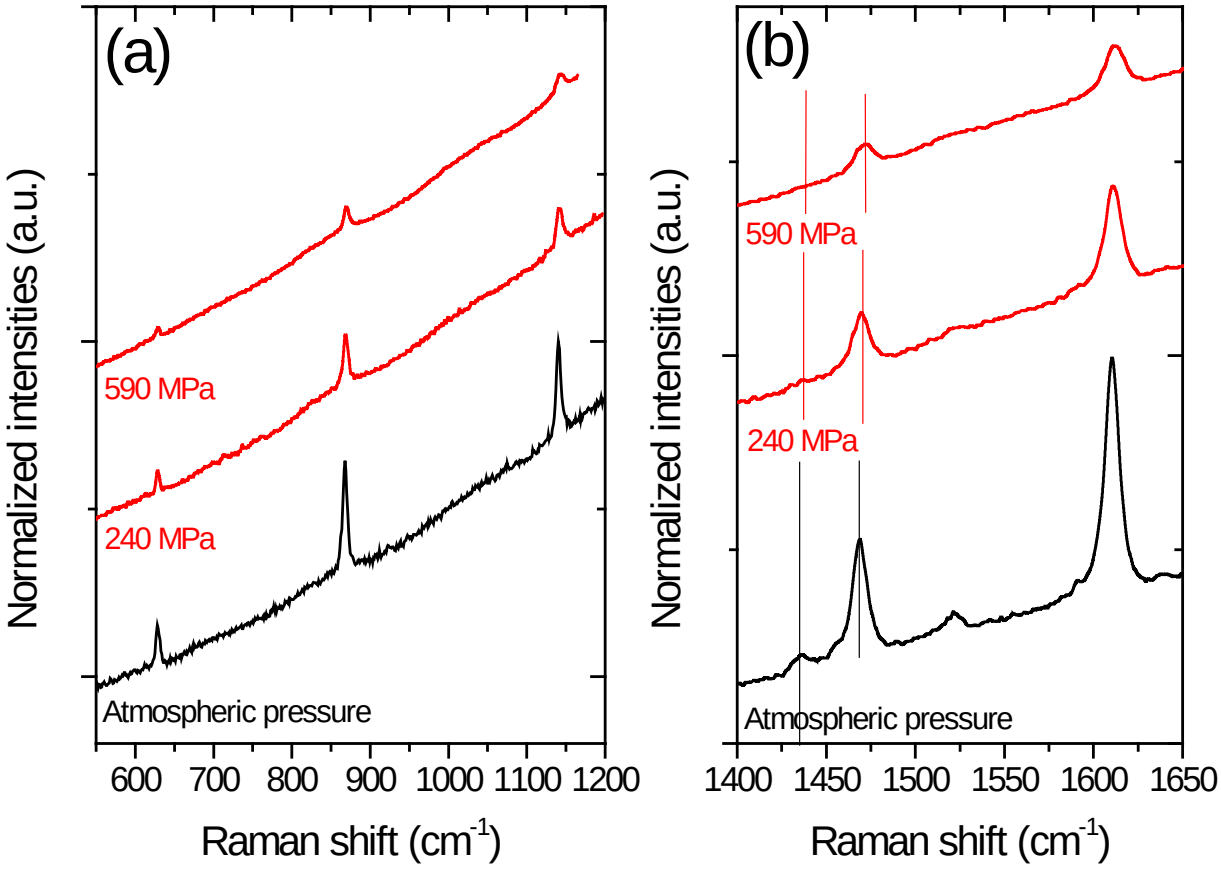

Figure S6 – Raman spectra recorded at λ=694 nm for the MIL-53(Al) as a function of the applied

pressure. (a): inorganic part, (b): organic part for compression. Mark bands show the shifts of characteristic bands during compression.

It was already established that in this family of materials, the band corresponding to the symmetric vibration of the carboxylate (ν_{sym}(COO)) can serve as a marker to detect the presence of the LP and the NP forms [10]. Figure S6.B shows that the ν_{sym}(COO) band initially centered around 1440 cm^{-1} shifts towards a lower wavenumber ~1430 cm^{-1} and disappear when increasing the pressure, consistent with a structural switching of the MIL-53(Al) from the LP to the CP forms as evidenced by Hg porosimetry and XRPD.

4. Molecular simulation

4.1. Molecular Dynamics

MD simulations were performed using the DL-POLY_1.9 program [11] in the NσT ensemble in order to take into account the possible change in size and shape of the MIL-53(Al) framework. The thermostat and anisotropic barostat of Berendsen were employed (with τ = 1.0 ps and τ = 5.0 ps as relaxation times) in order to maintain constant temperature and pressure during each MD simulation. Equations of motion were integrated using the velocity Verlet algorithms coupled with the QUATERNION, SHAKE-RATTLE algorithms. The MIL-53(Al) framework was described by the force field recently developed by Vanduyfhuys *et al.* [12]. A rescaling factor of 0.86 was applied to the Buckingham potential parameters. The simulation box consisted of 32 unit cells built from the crystallographic coordinates previously reported for the large pore form of MIL-53(Al) [13]. The MD simulations were run at 300 K under an external applied pressure in the range [0-200] MPa. Each calculation was performed for 5 ns with a time step of 1 fs (i.e. 5.10^6 steps) including 2 ns of equilibration. To further explore the structure behavior of the solid upon pressure release, the calculations were performed starting with the CP structure simulated at 200 MPa and by decreasing gradually the pressure.

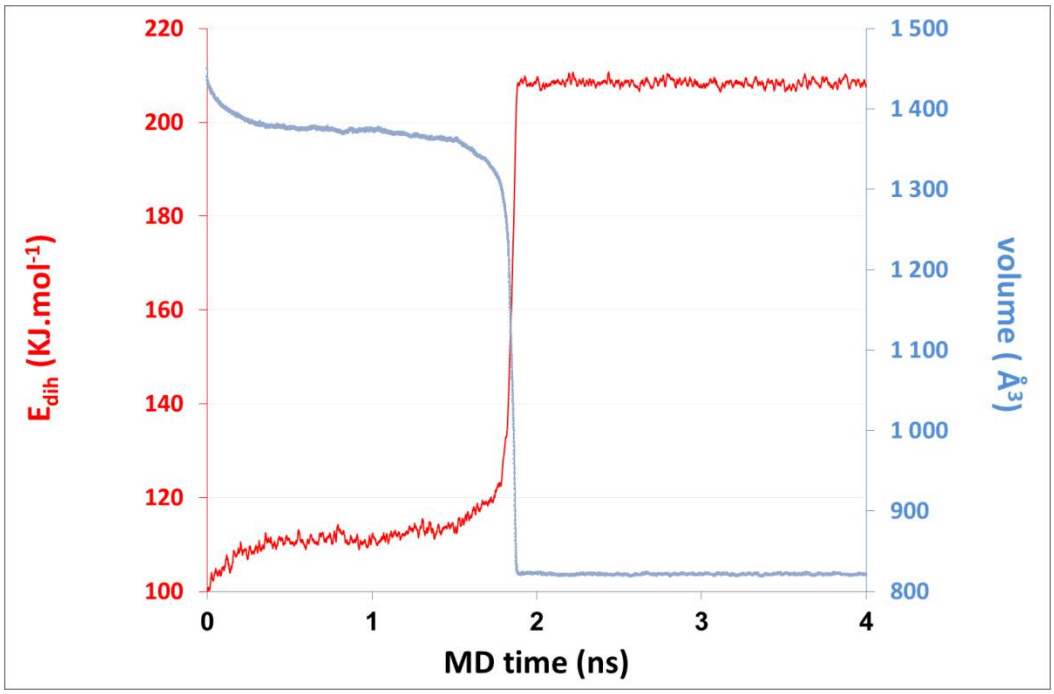

Figure S7: Evolution of the dihedral energy contribution (red) and of the unit cell volume (blue) as function of the MD simulation time starting with the LP form of MIL-53(Al) at 20 MPa.

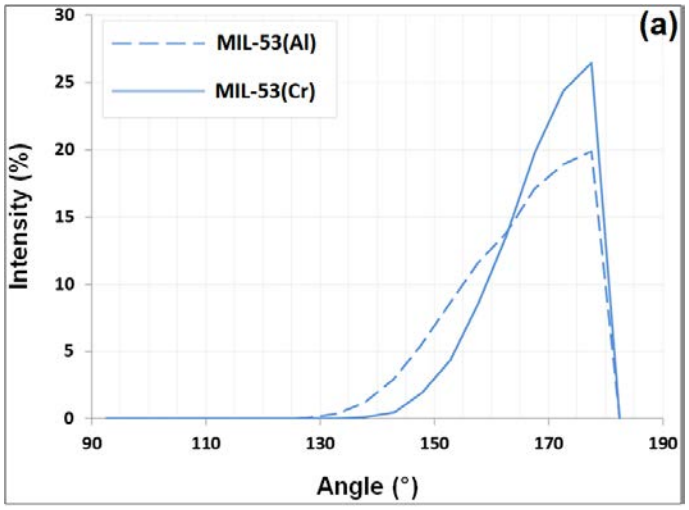

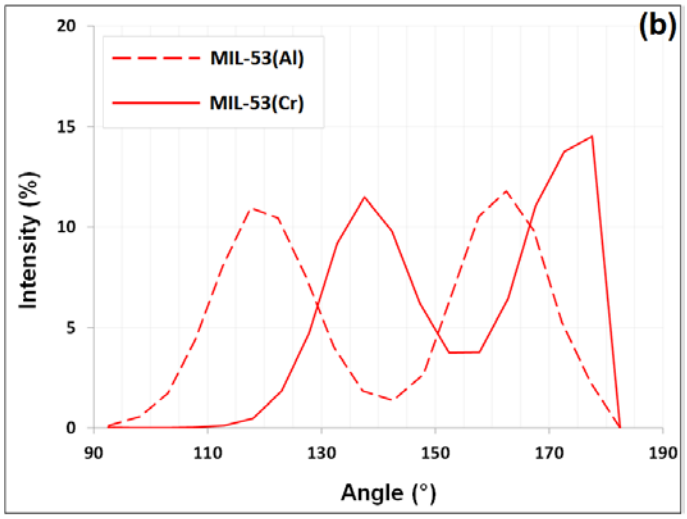

Figure S8: Comparison between the distribution of the torsion angle M-O_c-C_c-C_{g2} calculated for the LP (a) and the CP (b) forms of MIL-47(V^{IV}) and MIL-53(Al).

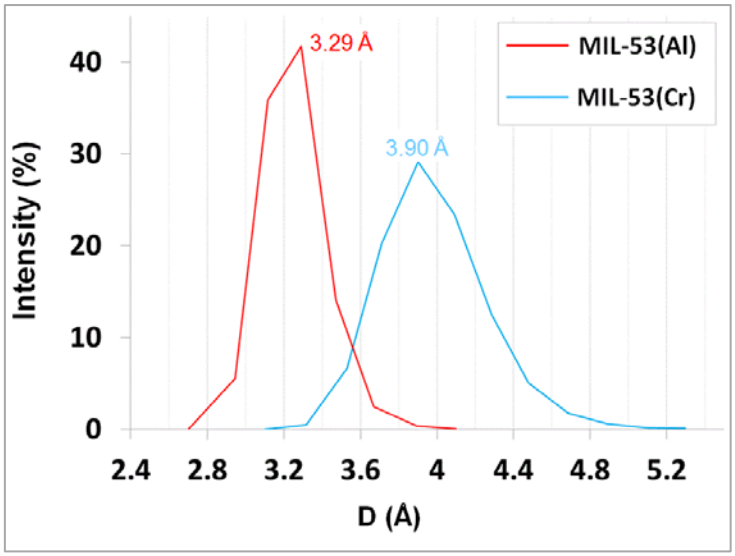

Figure S9: Distribution of the carbon-carbon distances separating the opposite phenyl rings in the CP forms of MIL-53(Al, Cr).

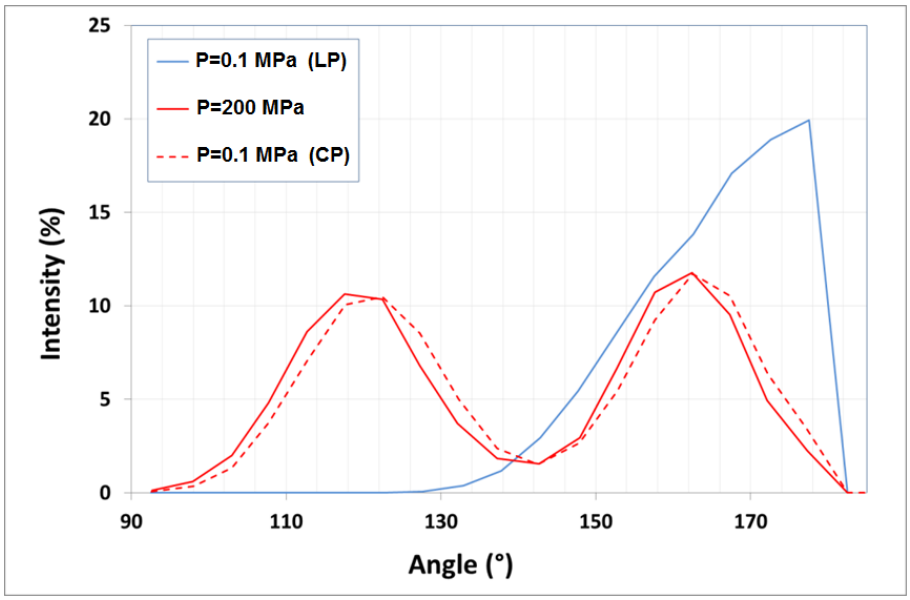

Figure S10: Comparison between the distributions of the torsion angle M-O_c-C_c-C_{g2} for the LP form obtained at 0.1 MPa (blue line), the CP form obtained at 200 MPa (continuous red line) and the CP form obtained at 0.1 MPa starting from the CP form at 200 MPa (dashed red line)

4.2. Volume scan

To computationally investigate the energy profile of MIL-53(Al) as function of volume, two scans were performed. The first scan consists of a series of constrained geometry optimizations during which the volume of the unit cell was kept fixed. The simulation reflects the behavior at 0K. The scan consists of 181 intermediate volumes chosen equidistantly between 700 A^3 and 1600 A^3. At each volume, a geometry optimization was performed in which the volume of the unit cell was kept fixed, while relaxing the nuclear coordinates and the shape of the unit cell. Next, the energy and pressure can be calculated for each volume (the pressure can be calculated from the virial tensor). By systematically repeating this procedure, it is possible to construct the energy and the pressure shown in Figure S12.

A second scan consists of separate NVT simulations (300 K) (in the Canonical ensemble) at each of the 181 intermediate volumes with a unit cell fixed to the 0 K value from the previous scan. Now the average internal energy and average pressure (from the virial tensor) can be calculated. The free energy can be calculated by integrating the pressure. All these profiles are shown in Figure S13.

Both scans were performed with the force field of Vanduyfhuys *et al.* [12] with a rescaling factor of 0.85 applied to the Buckingham potential parameters. The simulation box contained 2 unit cells along the direction of the AlO chain. The NVT simulations were done using the Langevin thermostat with a time constant of 100 fs, the time step of the Verlet algorithm was set to 1 fs and the total simulation time was 1 ns. Both scans were performed using Yaff, a force field simulation

package developed at the Center for Molecular Modeling [14].

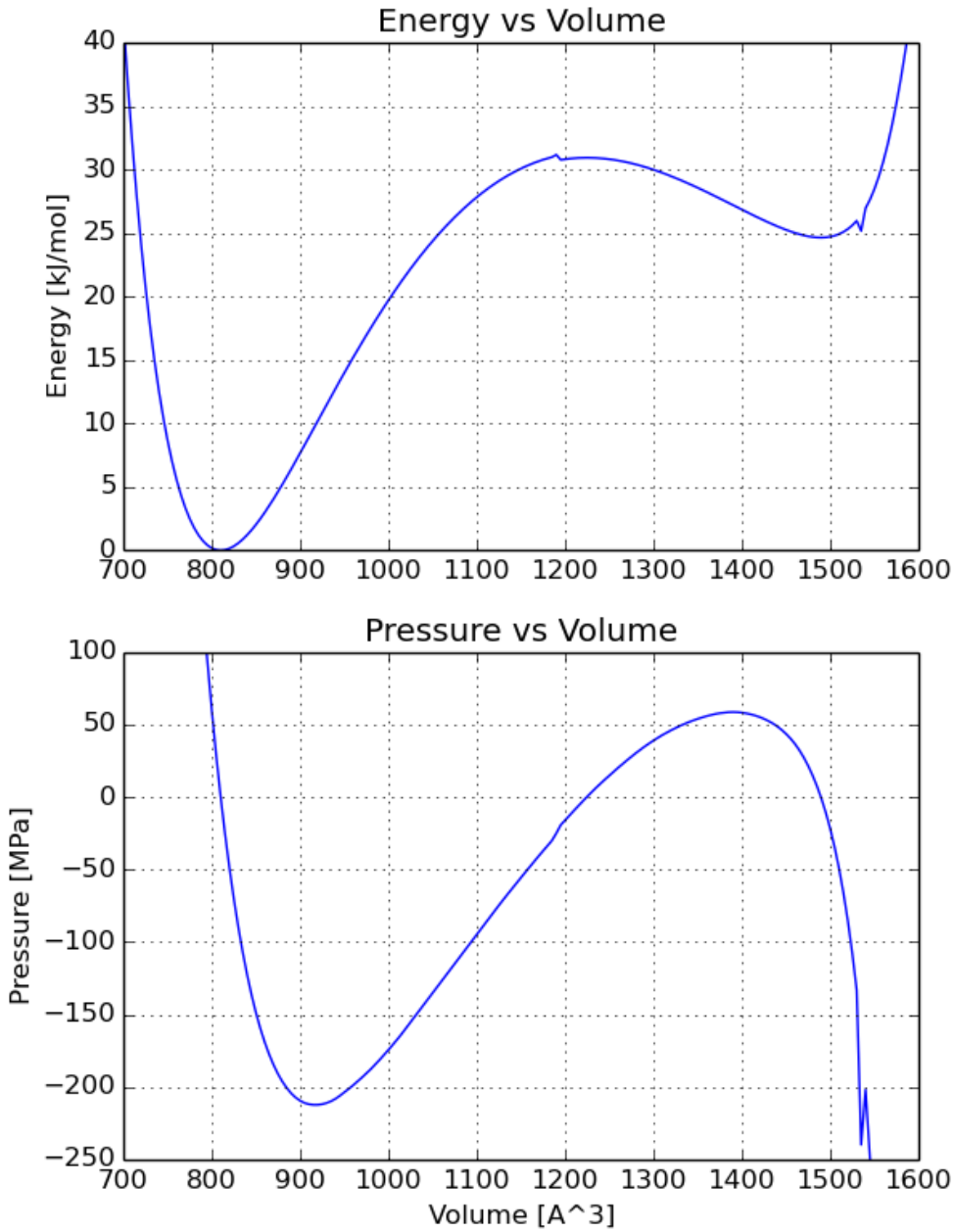

Figure S11: Energy and pressure profiles of MIL-53(Al) at 0 K

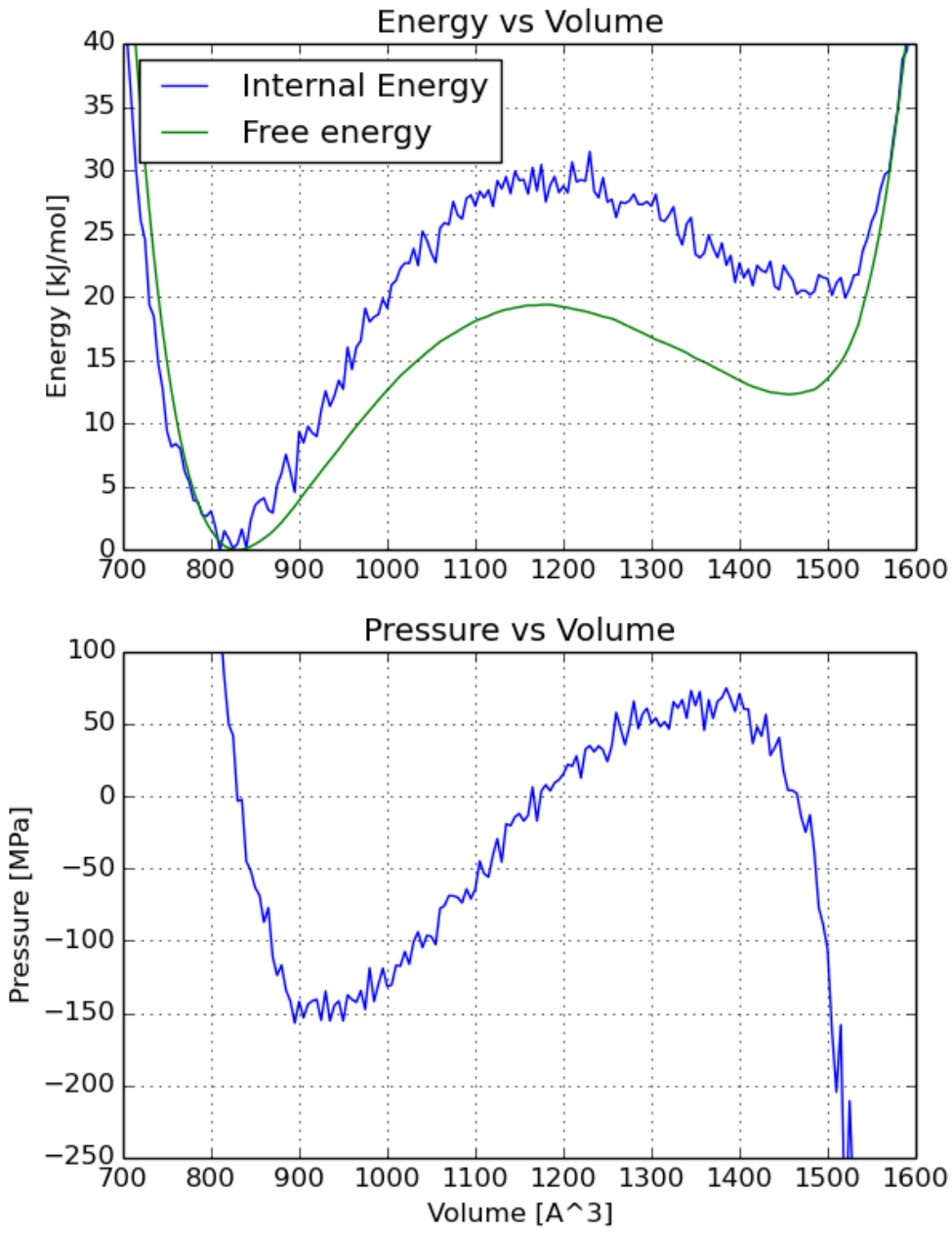

Figure S12: Free energy and pressure profiles of MIL-53(Al) at 300 K

References

[1] H. Giesche, *Part. Part. Syst. Charact.*, 2006, **23**, 9.

[2] I. Beurroies, M. Boulhout, P. L. Llewellyn, B. Kuchta, G. Férey, C. Serre, R. Denoyel, *Angew. Chem., Int. Ed.*, 2010, **49**, 7526.

[3] P.G. Yot, Q. Ma, J. Haines, Q. Yang, A. Ghoufi, T. Devic, C. Serre, V. Dmitriev, G. Férey, C. Zhong and G. Maurin, *Chem. Sci.*, 2012, **3**, 1100.

[4] R. P. Mayer, R. A. Stowe, *J. Colloid Sci.*, 1965, **20**, 893.

[5] W. Pabst, E. Gregorova, *Characterization of particles and particle systems*, ICT: Prague, 2007.

[6] A.V. Neimark,F.X. Coudert, C. Triguero, A. Boutin, A.H Fuchs, I. Beurroies, R. Denoyel, *Langmuir*, 2011, **27**, 4734.

[7] J. Rodriguez-Carvajal, A program for Rietveld refinement and pattern matching analysis. In Collected Abstracts of Powder Diffraction Meeting, 1990; pp 127.

[8] T. Roisnel, J. Rodriguez-Carvajal, In Abstracts of the 7th European Powder Diffraction Conference, Barcelona, Spain, 2000; p 71.

[9] H. K. Mao, J. Xu, P. M. Bell, *J. Geophys. Res.*, 1986, **91**, 4673.

[10] L. Hamon, P.L. Llewellyn, T. Devic, A. Ghoufi, G. Clet, V. Guillerm, G.D. Pirngruber, G. Maurin, C. Serre, G. Driver, W. van Beek, E. Jolimatre, A. Vimont, M. Daturi, G. Férey, *J. Am. Chem. Soc*. 2009, **131**, 17490.

[11] Smith, W. and Forester, T.R., J. Mol. Graphics, 1996, **14**,136.

[12] L. Vanduyfhuys, T. Verstraelen, M. Vandichel, M. Waroquier, and V. Van Speybroeck, *J. Chem. Theory Comput.* 2012, **8**, 3217.

[13] T. Loiseau, C. Serre, C. Huguenard, G. Fink, F. Taulelle, M. Henry, T. Bataille, G. Férey, *Chem. Eur. J*. 2004, **10**, 1373.

[14] T. Verstraelen, L. Vanduyfhuys, S. Vandenbrande, *Yaff, yet another force field*, http://molmod.ugent.be/software/.